



EXPRES. I. HD 3651 as an Ideal RV Benchmark

John M. Brewer¹, Debra A. Fischer², Ryan T. Blackman², Samuel H. C. Cabot², Allen B. Davis², Gregory Laughlin², Christopher Leet², J. M. Joel Ong (王加冕)², Ryan R. Petersburg², Andrew E. Szymkowiak², Lily L. Zhao², Gregory W. Henry³, and Joe Llama⁴

¹ Department of Physics and Astronomy, San Francisco State University, 1600 Holloway Ave., San Francisco, CA 94132, USA; jmbrewer@sfsu.edu

² Department of Astronomy, Yale University, 52 Hillhouse Ave., New Haven, CT 06511, USA

³ Center of Excellence in Information Systems, Tennessee State University, Nashville, TN 37209 USA

⁴ Lowell Observatory, 1400 Mars Hill Rd., Flagstaff, AZ 86001, USA

Received 2020 May 8; revised 2020 June 2; accepted 2020 June 2; published 2020 July 16

Abstract

The next generation of exoplanet-hunting spectrographs should deliver up to an order of magnitude improvement in radial velocity (RV) precision over the standard 1 m s^{-1} state-of-the-art spectrographs. This advance is critical for enabling the detection of Earth-mass planets around Sun-like stars. New calibration techniques such as laser frequency combs and stabilized etalons ensure that the instrumental stability is well characterized. However, additional sources of error include stellar noise, undetected short-period planets, and telluric contamination. To understand and ultimately mitigate error sources, the contributing terms in the error budget must be isolated to the greatest extent possible. Here, we introduce a new high-cadence RV program, the Extreme Precision Spectrograph (EXPRES) 100 Earths Survey, which aims to identify rocky planets around bright, nearby G and K dwarfs. We also present a benchmark case: the 62 day orbit of a Saturn-mass planet orbiting the chromospherically quiet star, HD 3651. The combination of high eccentricity (0.6) and a moderately long orbital period ensures significant dynamical clearing of any inner planets. Our Keplerian model for this planetary orbit has a residual rms of 58 cm s^{-1} over a ~ 6 month time baseline. By eliminating significant contributors to the RV error budget, HD 3651 serves as a standard for evaluating the long-term precision of extreme precision RV programs.

Unified Astronomy Thesaurus concepts: Planet hosting stars (1242); Radial velocity (1332); Exoplanet dynamics (490); Exoplanet astronomy (486)

Supporting material: machine-readable table

1. Introduction

Following the early detections of gas giant planets around Sun-like stars, radial velocity (RV) surveys saw a steady stream of discoveries, punctuated by regular improvements in instrumental precision. With the introduction of the environmentally stabilized High Accuracy Radial velocity Planet Searcher (HARPS) spectrograph in 2003 (Mayor et al. 2003), single-measurement RV precision reached $\sim 1 \text{ m s}^{-1}$. Multi-decade campaigns continued to push to lower mass planets and longer period orbits, but the state-of-the-art RV precision (Fischer et al. 2016) has remained at this level for more than a decade.

The long-term nature of RV surveys has enabled the collection of thousands of high-fidelity measurements for a range of spectral types. Many of these stars are RV standards without detected planets. The RV rms scatter of standard stars or the residuals after fitting a simple Keplerian model has been used to evaluate RV measurement precision. The quietest stars have shown a scatter of just under $\sim 2 \text{ m s}^{-1}$ (Huang et al. 2018; Soubiran et al. 2018; Brems et al. 2019). However, it is unclear how this RV scatter is apportioned between astrophysical, instrumental, and analysis error sources.

The Kepler and K2 transit surveys have demonstrated that nearly every star hosts at least one planet (Burke et al. 2015; Hsu et al. 2018). The most commonly detected transiting planet has a radius between 1 and $4 R_{\oplus}$ (Burke et al. 2015) and many of the transiting planet architectures contain tightly packed systems of small planets (Winn & Fabrycky 2015) that would produce short-period, low-amplitude reflex velocities in the

host stars. Analogs of the Kepler rocky planets and compact multiplanet systems are largely missing from RV surveys. This implies that at least some of the RV scatter in standard stars is likely caused by undetected low-mass planets. Both improved RV precision and higher observing cadence are required to tease out these signals. Since a reliable sample of stars without planets does not exist, a new type of standard star is needed to evaluate improvements in RV precision.

The Extreme Precision Spectrometer (EXPRES) is one of the first in a new generation of Extreme Precision Radial Velocity (EPRV) instruments delivering high-fidelity data with the goal of disentangling photospheric velocities from Keplerian velocities. EXPRES is located at the Lowell Discovery Telescope (LDT; Levine et al. 2012; DeGroot et al. 2014). The instrumental stability is at least 10 cm s^{-1} (Blackman et al. 2020) with single-measurement uncertainties of about 30 cm s^{-1} in spectra with a signal-to-noise ratio (S/N) ~ 250 per pixel at 550 nm (Petersburg et al. 2020). The primary science mission for EXPRES is the 100 Earths Survey to identify low-mass planets in habitable zone orbits around Sun-like stars. The combination of high-precision measurements and high observing cadence will enable the detection of planets that were commonly found with the Kepler mission, but that have been missed in previous RV surveys.

In this paper, we highlight our RV data for HD 3651 b as a way to evaluate the long-term, on-sky precision of EPRV instruments. The high eccentricity of this planetary orbit dynamically clears out most simulated test particles within and slightly outside its orbit, as expected from stability theory (Gladman 1993). Similar orbital parameters are known for only

a handful of detected exoplanets. HD 3651 is especially well suited as a standard star for demonstrating RV precision because this bright star is accessible by all current EPRV instruments.

2. EXPRES

EXPRES was fully commissioned in 2019 February and has been used to collect science observations for the 100 Earths Survey since that time. The high-resolution optical spectrograph is a fiber-fed echelle design (Jurgenson et al. 2016) with double scrambling and active agitation (Petersburg et al. 2018). It covers 3800–7800 Å and has a median resolving power of $R = 137,500$. EXPRES is located in a vibration isolated vacuum enclosure, in a temperature controlled room. The front-end module contains an atmospheric dispersion compensator and a fast tip-tilt system keeps the star focused on the 0".9 octagonal input fiber. The overall seeing-dependent throughput is $\sim 8\%$ – 15% (Blackman et al. 2020). Wavelength calibration is carried out with a Menlo Systems laser frequency comb (LFC; Probst et al. 2016), and we have demonstrated an instrumental precision better than 10 cm s^{-1} (Blackman et al. 2020). A chromatic exposure meter picks off 2% of the light to monitor photon arrival times (Blackman et al. 2017, 2019). The current single-measurement precision is 30 cm s^{-1} at S/N of 250 per pixel (Petersburg et al. 2020), meeting the spectrograph design goals. Further work is underway to mitigate the impact of photospheric noise on the RVs. All instrument adjustments and observations are handled through a python-based messaging server and associated database with a web front-end, enabling high-cadence observations with minimal overhead.

2.1. The Science Goals

The primary mission for EXPRES is the 100 Earths Survey, which will search for low-mass planets with orbital radii stretching out to the habitable zones of Sun-like stars. These discoveries will reach a new parameter space for RV surveys by detecting planets that are more likely to have habitable conditions orbiting nearby stars. Furthermore, the discovery of lower mass planets will help to reconcile the currently discrepant results between transit and RV searches. The science goals of EXPRES will be achieved by combining high-precision, high-cadence observations with a long-term monitoring program at the LDT. EXPRES can also be used for follow-up of transiting planets around bright stars discovered with the Transiting Exoplanet Survey Satellite (TESS) mission (Ricker et al. 2015) and the instrument is being used to characterize exoplanet atmospheres with high-dispersion spectroscopy (Hoeijmakers et al. 2020).

2.2. Stellar Targets for the 100 Earths Survey

The primary targets for the 100 Earths Survey include 66 G and K dwarfs distributed over the northern sky; most of these stars are brighter than $V \sim 7$ (Table 1) and were selected to be chromospherically quiet, without detected gas giant planets. A few stars with high chromospheric activity or known planets were also included; these stars serve as benchmarks to evaluate the on-sky performance of the program. They allow us to search for low-mass planetary companions to known gas giants, and they provide excellent data sets for developing statistical mitigation strategies for stellar activity.

Table 1
Primary Targets for the First Phase EXPRES Survey

HD	Sp. Type	Vmag	P-mode (s)
3651	K0V	5.88	273
4628	K2V	5.74	236
9407	G6V	6.53	350
10476	K1V	5.24	260
10700	G8V	3.50	258
16160	K3V	5.5	220
18803	G8V	6.4	296
19373	G0V	3.8	340
22049	K0V	3.72	150
26965	K1V	4.43	258
32147	K3V	6.21	215
34411	G0V	4.8	492
38858	G4V	5.97	306
50692	G0V	5.75	365
52711	G4V	5.95	350
55575	G0V	5.6	428
69830	K0V	5.95	284
71148	G5V	6.3	406
75732	G8V	5.95	370
76151	G3V	6.0	330
84737	G2V	5.1	710
86728	G1V	5.4	433
89269	G5V	6.65	346
95128	G0V	5.04	450
95735	M2V	7.5	254
99491	K0V	6.5	200
99492	K3V	7.5	190
101501	G8V	5.34	260
103095	K0V	6.45	182
104304	K0V	5.55	396
105631	K0V	7.5	280
110897	G0V	5.95	290
114783	K0V	7.55	270
115617	G6.5 V	4.74	316
117043	G6V	6.2	318
122064	K3V	6.52	200
126053	G1.5 V	6.3	310
127334	G5V	6.36	472
136923	G9V	7.1	240
141004	G0V	4.42	540
143761	G0V	5.2	384
146233	G2V	5.5	420
154345	G8V	6.6	260
157214	G0V	5.39	220
157347	G5V	6.28	335
158259	G0V	6.5	222
158633	K0V	6.43	220
159222	G1V	6.4	300
161797	G5IV	3.4	700
164922	G9V	6.8	240
166620	K2V	6.4	255
168009	G2V	6.3	416
182488	G8V	6.36	325
185144	K0V	4.68	232
186408	G2V	5.95	465
186427	G5V	6.2	380
190404	K1V	7.3	220
190406	G1V	5.8	458
191785	K0V	7.3	220
193664	G3V	5.75	333
197076	G5V	6.44	340
199960	G1V	6.2	480
210277	K0V	8.57	397
217014	G2V	5.5	422

Table 1
(Continued)

HD	Sp. Type	Vmag	P-mode (s)
218868	K0V	7.0	330
219134	K3V	5.57	210
221354	K2V	6.76	285

2.3. Exposure Times

The detection of low-mass planets orbiting in the stellar habitable zone requires high S/N observations. Petersburg et al. (2020) show that the EXPRES single-measurement RV errors decrease with increasing S/N, dropping from errors of about 90 cm s^{-1} for S/N ~ 100 (per pixel at 550 nm) to about 30 cm s^{-1} for S/N of 250. At S/N > 250 , the curve flattens with minimal gains in RV measurement precision. To minimize spurious velocity shifts due to charge transfer inefficiency (Blackman et al. 2020), all stars are observed at a consistent S/N, and based on our analysis of the dependence of RV error on S/N for our target stars, we have set this to be S/N = 250 per pixel at 550 nm. This S/N is well below the saturation of the detector and with the 4 pixel line-spread function (LSF) of EXPRES; this yields S/N = 500 per resolution element for each exposure. To ensure that we reach a perfectly “baked” level in our spectra, our chromatic exposure meter picks off a fraction of the light entering the spectrograph and counts photons in the V band. The exposure meter counts have been calibrated to measured S/N in the extracted spectra and the exposure meter terminates the exposure when one of the following conditions is met: either an S/N of 250 has been reached or 20 minutes have elapsed (whichever comes first). The 20 minute limit for exposure times is set to minimize errors in the chromatic barycentric correction (Blackman et al. 2019). For most stars, the resulting exposure times span or exceed the peak period of the p-mode oscillations (Chaplin et al. 2019). For brighter stars, additional observations are obtained to average over p-mode oscillations and for very faint stars additional observations are needed to reach our desired S/N.

2.4. Cadence

We initially started the 100 Earths Survey with four consecutive observations for every target. After we had accumulated a 6 month data set, we randomly removed one of the four observations and found that when we refit our data there was almost no increase in the residual velocity rms. With our 4 pixel LSF, three consecutive observations of spectra still yields an S/N of $250 \times \sqrt{4} \times \sqrt{3} = 866$ per resolution element in the nightly binned data, and reducing the number of consecutive observations from four to three has the important benefit that more targets can be covered each night. Therefore, every target on the 100 Earths Survey is now observed three times per night, each time it has been scheduled, weather permitting. Under the assumption of white noise, three exposures should improve the single-measurement precision of 30 cm s^{-1} to a nightly binned measurement precision of $\sim 17 \text{ cm s}^{-1}$. To track any small instrumental drifts in the wavelength solution during the night, science observations are interspersed with LFC frames every 15–30 minutes. The 10 s LFC observations have a readout time of 27 s and are generally taken during telescope slew times, so very little time

(no more than about 10 minutes per full night) is lost taking these calibrations. The 100 Earths Survey is currently allocated up to 70 nights yr^{-1} on the 4.3 m LDT. Most of these nights are scheduled as half or quarter nights to maximize cadence on the target stars.

2.5. Data Reduction and Analysis

The EXPRES analysis pipeline uses a flat-relative optimal extraction algorithm (Petersburg et al. 2020). Each night, 30 dark and 30 science flat images are taken and used to reduce and extract the science frames. Order tracing is accomplished using the reduced science flats and after a scattered light model is removed, the flat-relative optimal extraction is performed. Wavelength solutions are interpolated from bracketed LFC images taken throughout the night and a nightly exposure of a Thorium Argon calibration lamp is used as a calibration reference to initiate the LFC wavelength solution. The chromatic, flux-weighted midpoint time is calculated from the exposure meter data stored in a FITS header table with each spectrum. After telluric line identification and masking is done using a self-calibrating, empirical, linear regression telluric model, SELENITE (Leet et al. 2019), and the absolute RVs are derived using a forward model (Petersburg et al. 2020).

2.6. Validating On-sky Precision

EXPRES has met its design specifications (Blackman et al. 2020). Petersburg et al. (2020) showed that Keplerian fitting of 47 observations for 51 Peg b yielded orbital parameters consistent with literature values with an rms scatter in the residual velocities of 88 cm s^{-1} . This indicates that there is residual RV scatter from some combination of the stellar photosphere, the instrument, and our analysis pipeline. It is common, especially when testing new instruments or analyses, to choose a standard star to evaluate the RV performance. However, an improvement in precision can mean that previously well-characterized stars may reveal surprises. Given that we expect low-amplitude, high-frequency signals (i.e., small rocky planets, compact systems) around a significant fraction of stars (Winn & Fabrycky 2015), some of RV standard stars may harbor planets in the RV noise. It would be helpful to have even one case where we could be sure that additional planets were not contributing to the residual RV scatter.

3. HD 3651: An EPRV Calibrator

To evaluate our measurement precision, we wanted to rule out contamination from low-amplitude, short-period planets. Instead of focusing on RV quiet stars, we selected a star with a known planet in a very eccentric and moderately long-period orbit. Our simulations show that short-period planets should not be able to survive (Section 5), leaving the exoplanetary system free of RV scatter from undetected exoplanets.

HD 3651 is an old nearby K dwarf with stellar parameters summarized in Table 2. The star hosts a Saturn-mass planet ($M \sin i \sim 70 M_{\oplus}$) on a ~ 62 day orbit with an eccentricity of 0.61. Since its discovery (Fischer et al. 2003), additional observations have been obtained using the Keck High Resolution Echelle Spectrometer (HIRES; Butler et al. 2017). Using 161 archival observations taken over 17 yr, we fit a single-planet model to the data with an rms scatter to the residuals of 3.4 m s^{-1} (Table 4). This is a few times larger than

Table 2
HD 3651 Parameters

Parameter	Value
Identifier	54 Psc HR 166 HIP 3093
V mag	5.88
$B-V$	0.85
dist (pc)	11.137 (0.007)
L	0.52
M_V	6.11
Sp Type	K0V
Age (Gyr)	8.2 (3.0)
T_{eff} (K)	5210 (30)
$\log g$	4.45 (0.15)
[Fe/H]	0.05 (0.05)
$v \sin i$ (km s $^{-1}$)	1.7 (0.5)
Mass (M_{\odot})	0.8 (0.05)
Radius (R_{\odot})	0.88 (0.02)
RV (km s $^{-1}$)	−33.00 (0.16)
$\log R'_{\text{HK}}$	−5.01
P_{rot} (days)	44.5

the single-measurement precision of HIRES and close to the low end of the distribution of RV rms scatter for Keck HIRES (Fischer et al. 2016). The low activity of the star ($R'_{\text{HK}} = -5.01$) makes this an ideal target with low intrinsic stellar jitter (Isaacson & Fischer 2010). The rms in the HIRES RV residuals suggests that instrumental or analytical uncertainties may dominate the error budget. For comparison, Cosentino et al. (2014) found that a single-planet fit to two years of data using the HARPS-N spectrograph gave an rms scatter of 1.82 m s $^{-1}$ for HD 3651.

3.1. Observations

We obtained 61 EXPRES RV measurements between 2019 August and 2020 February, which are presented in Table 3. The velocities were derived from optimally extracted spectra with forward modeling, as described in Petersburg et al. (2020). A histogram showing the distribution of tabulated single-measurement errors is shown in Figure 1. The relatively high cadence of the 100 Earths Survey allowed for excellent phase coverage over two orbital periods for HD 3651 b. On a night when we did not have telescope time, Lowell astronomer Maxime Devogele kindly yielded about 20 minutes of his time so that we could obtain a set of four spectra that allowed us to catch the rapid velocity change during periastron passage in 2019 November.

3.2. Keplerian Fitting

Keplerian modeling of the velocities for HD 3651 was carried out using a Levenburg–Marquardt algorithm to fit the linearized Keplerian equations (Wright & Howard 2009) that are built into the IDL widget Keplerian Fitting Made Easy developed by Giguere et al. (2012). The best-fit model yields an orbital period of 61.88 ± 0.55 days, consistent with the better constrained orbital period of 62.26 ± 0.075 days modeled with the 17 yr time baseline of Keck HIRES data (Butler et al. 2017). Fixing the orbital period to 62.26 days gives an equally good fit in the EXPRES data (Figure 2) with a residual velocity rms of 58 cm s $^{-1}$. There is no apparent

Table 3
EXPRES RVs of HD 3651

BJJD	Vel (m s $^{-1}$)	Err (m s $^{-1}$)
18714.482110	−10.090	0.329
18714.490311	−9.811	0.334
18715.476876	−11.452	0.377
18715.485466	−11.262	0.396
18716.417348	−12.623	0.311

(This table is available in its entirety in machine-readable form.)

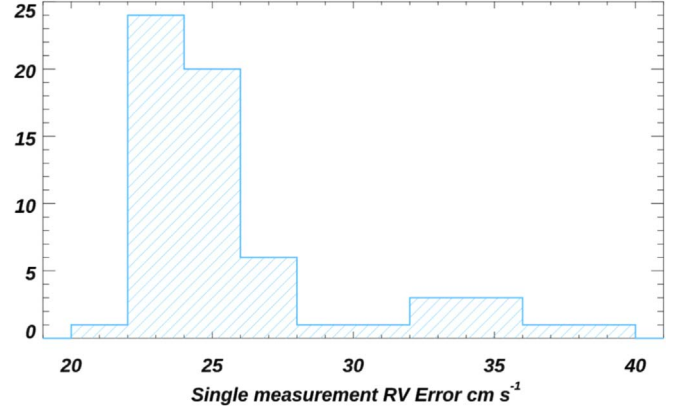


Figure 1. Distribution of single-measurement errors for HD 3651 with EXPRES spectra obtained between 2019 August and 2020 February. These unbinned measurement uncertainties are typically about 25 cm s $^{-1}$.

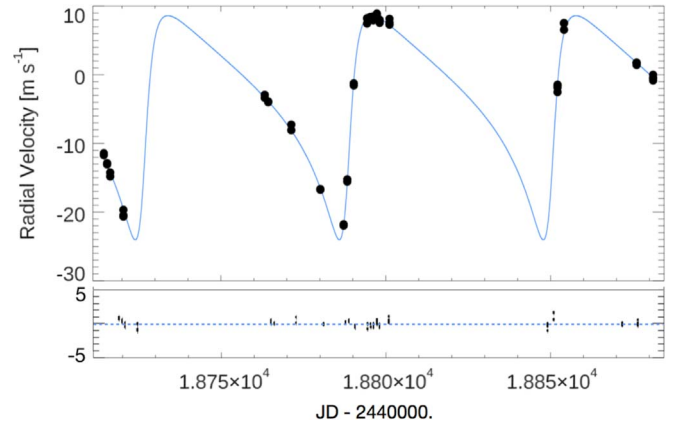


Figure 2. The time-series RV measurements of HD 3651 are fitted with a Keplerian model (shown with the blue curve). The residual velocities to this fit have an rms of 58 cm s $^{-1}$.

periodicity in the residuals and a Lomb–Scargle periodogram shows no significant peaks.

To obtain uncertainties in the orbital parameters, we ran 1000 bootstrap Monte Carlo (MC) trials. For each MC trial, we fit a Keplerian orbit to the data, subtracted the best-fit model, scrambled the residuals (seeding with a random number generator), and added the scrambled residuals back to the best-fit model Keplerian velocities. We also carried out 1000 bootstrap MC trials with the Keck HIRES data (Butler et al. 2017). The bootstrap MC errors on the orbital period and the time of periastron passage were smaller with the Keck HIRES data set because of the longer time baseline; however, the errors on all other orbital parameters were somewhat larger with the Keck HIRES data because of the larger error bars on those RV measurements. The independently fit model parameters for

Table 4
Keplerian Model for HD 3651 b

Parameter (1)	EXPRES (2)	Keck HIRES (3)
P (days)	61.88 ± 0.55	62.26 ± 0.075
T_p (days)	58726.2 ± 1.2	58726.68 ± 0.5
e	0.606 ± 0.09	0.612 ± 0.12
ω	243.8 ± 23.4	231.9 ± 41
K (m s $^{-1}$)	16.93 ± 0.22	17.15 ± 0.9
$M \sin i$ (M_J)	69.04 ± 4.1	66.88 ± 5.9
a_{rel} (au)	0.284 ± 0.002	0.285 ± 0.001
RMS (m s $^{-1}$)	0.58	3.4

HD 3651 b using EXPRES and HIRES data are summarized in Table 4.

The phased orbital fit for the EXPRES velocities is shown in Figure 3 where we also include the fit to the archival Keck data phased and plotted in the same way for comparison. The EXPRES data show much less scatter in the RVs with scatter in the residuals that is about six times smaller than the Keck HIRES data.

4. Automatic Photoelectric Telescope Photometric Observations

To analyze the variability and look for serendipitous transits of the planet, we present 1192 photometric observations of HD 3651 acquired over an interval of 25 yr from the 1993–1994 to the 2017–2018 observing seasons with the T4 0.75 m Automatic Photoelectric Telescope (APT) at Fairborn Observatory in southern Arizona. Our observations include the 10 observing seasons presented in the HD 3651b discovery paper of Fischer et al. (2003). The T4 APT is equipped with a single channel photometer that uses an EMI 9124QB bi-alkali photomultiplier tube to measure the difference in brightness between the program star and three nearby comparison stars in the Strömgren b and y passbands. To improve the photometric precision, we combine the differential b and y magnitudes into a single $(b + y)/2$ passband. The precision of a single observation with T4, as measured from pairs of constant comparison stars, is around 0.0015 mag on good nights. The T4 APT is described in Henry (1999), where further details of the telescope, precision photometer, and observing and data reduction procedures can be found.

Table 5 gives a summary of the photometric results of HD 3651. We computed the differential magnitudes in the sense HD 3651 minus HD 3690, the best of our three comparison stars. All magnitudes in the table refer to the average $(b + y)/2$ passband. The standard deviations of a single observation from the seasonal means, given in column 4, range from 0.00105 to 0.00197 mag, so the night-to-night scatter in the observations is similar to the typical measurement uncertainty. Period analysis found no significant variability within any observing season. However, the seasonal means given in column 5 exhibit a range of ~ 0.003 mag. HD 3651 is a quiet star with a very low value of $\log R'_{\text{HK}} = -5.01$ and so probably exhibits no spot variability measurable at our precision. The K0 Iab comparison star is the likely source of the long-term variability.

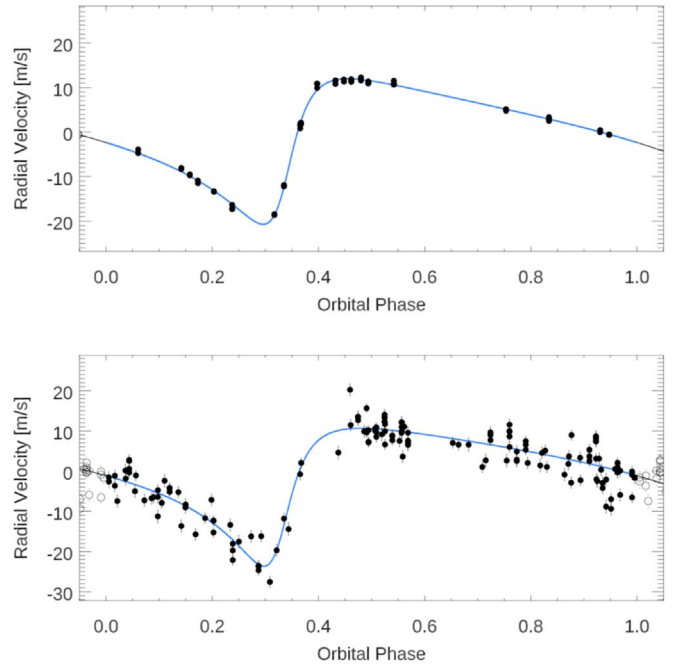


Figure 3. Phased RVs, Keplerian orbital fits, and residuals for observations of HD 3651b obtained with EXPRES (top) and Keck archival data (bottom) from Butler et al. (2017). The rms to the residuals for the EXPRES data is 0.58 m s^{-1} , compared to 3.46 m s^{-1} rms for the Keck HIRES data.

Table 5
APT Photometric Observations for HD 3651

Obs Season	N_{obs}	Date Range HJD-2,400,000	Sigma (mag)	Seasonal Mean (mag)
1993–94	22	49258–49382	0.00105	0.41059(22)
1994–95	22	49633–49750	0.00127	0.41078(27)
1995–96	24	49904–50084	0.00124	0.41128(25)
1996–97	22	50391–50480	0.00150	0.41170(32)
1997–98	51	50718–50856	0.00153	0.41118(21)
1998–99	61	51080–51218	0.00140	0.41111(17)
1999–00	69	51434–51586	0.00141	0.41129(19)
2000–01	57	51805–51952	0.00141	0.41129(19)
2001–02	41	52193–52317	0.00149	0.41182(23)
2002–03	52	52448–52673	0.00158	0.41147(22)
2003–04	71	52897–53048	0.00150	0.41121(18)
2004–05	69	53183–53405	0.00149	0.41063(18)
2005–06	74	53557–53778	0.00163	0.41033(19)
2006–07	70	53913–54140	0.00165	0.41122(20)
2007–08	54	54275–54502	0.00173	0.40952(23)
2008–09	63	54728–54865	0.00134	0.41040(17)
2009–10	45	55091–55222	0.00171	0.41106(25)
2010–11	55	55374–55595	0.00135	0.41110(18)
2011–12	43	55830–55960	0.00144	0.41215(22)
2012–13	56	56185–56315	0.00177	0.41201(24)
2013–14	60	56468–56680	0.00181	0.41171(23)
2014–15	35	56833–57043	0.00197	0.41127(33)
2015–16	29	57296–57414	0.00190	0.41023(35)
2016–17	20	57673–57784	0.00182	0.41006(41)
2017–18	27	57933–58147	0.00159	0.40874(31)

4.1. APT Photometric Analysis

For further analysis, the 25 observing seasons of APT photometry are normalized such that all 25 seasons have the same mean magnitude as the first. This removes the long-term variability in the comparison star and in HD 3651, if any. The

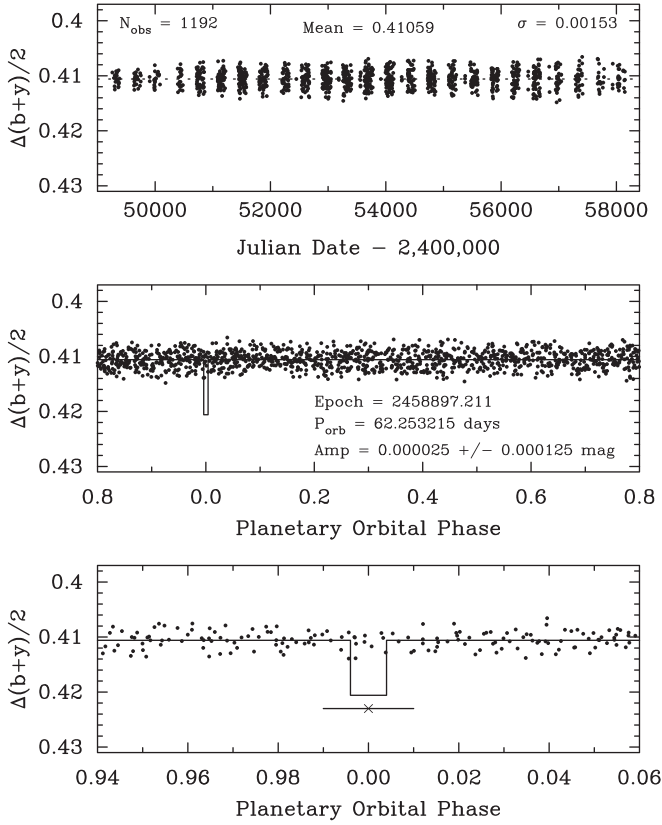


Figure 4. Photometric observations of HD 3651 acquired over 25 yr with the T4 0.75 m APT at Fairborn Observatory. Top: normalized observations show a scatter of 0.00153 mag from the mean, consistent with the measurement precision of the T4 APT. Middle: normalized observations phased with the orbital period of HD 3651 b show an upper limit of any variability on the orbital period of 25 ppm. Bottom: the normalized observations around the predicted phase of transit show no evidence for a transit. The point below the transit model shows the predicted time of transit center and its 1σ uncertainty.

1192 normalized observations are plotted in the top panel of Figure 4, where we note that the standard deviation of all observations from the normalized mean is 0.00153 mag, consistent with our measurement precision. A period search of the complete normalized data set shows no significant variability between 1 and 100 days, as expected from HD 3651’s low value of $\log R'_{\text{HK}}$ and the low scatter in the observations. In particular, we find no signal in the vicinity of the estimated 44.5 day rotation period from Fischer et al. (2003).

The observations are phased with the epoch of transit center and the orbital period of the planet and are plotted in the middle panel of the figure. A least-squares sine fit of the normalized observations to the planetary orbital period gives a peak-to-peak amplitude of 0.000025 ± 0.000125 mag. This extremely low limit to any variability on the planetary orbital period is strong confirmation that the observed Doppler shifts are due to the planetary reflex motion of HD 3651 b.

Finally, in the bottom panel of Figure 4, we show the photometric observations near the transit epoch predicted from the RVs. Given the orbital period and orientation of the orbit, the transit probability is only about 1%. The transit duration is computed from the orbital elements and properties of the star, while the transit depth is estimated to be around 0.01 mag. The horizontal error bar below the transit window is the uncertainty

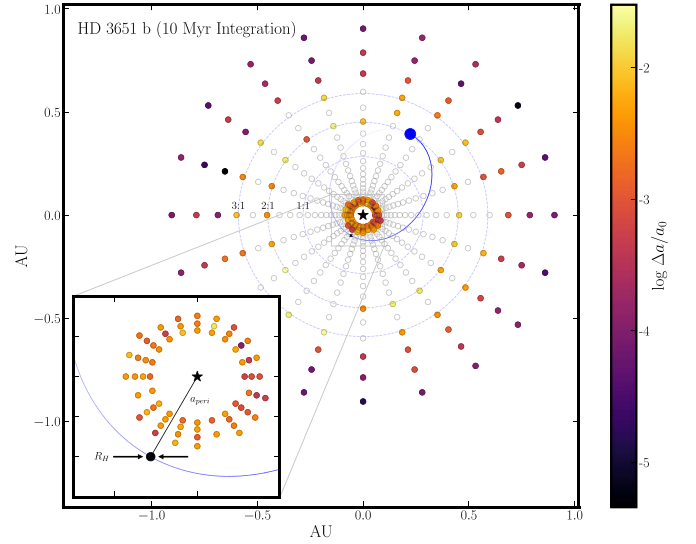


Figure 5. Orbital stability of zero-mass test particles placed at the starting locations shown. The color scale indicates the fractional change in semimajor axes over the length of the integration, with darker colors representing more stable initial orbits. The inset shows planets interior to HD 3651b that are able to survive for the entire simulation, with the planet’s Hill radius shown for reference. All particles show some change in their orbital parameters over only 10 Myr. Empty circles indicate initial positions of particles that suffered collision with the planet or star, or ejection from the system. We also mark circular orbits with 1:1, 2:1, and 3:1 mean-motion resonance with HD 3651 b.

in the time of transit. It is clear there remains no evidence for transits of HD 3651 b.

5. Dynamical Clearing from HD 3651 B

From the photometric observations, we can see that HD 3651 is a chromospherically inactive star. The high-eccentricity planet also makes it unlikely that there are interior planets that might contribute to additional low-amplitude, high-frequency noise in RV fitting. We test the stability of various orbits using *N*-body simulations of the HD 3651 b system. We use the MERCURIUS hybrid symplectic integrator included in the REBOUND package (Rein et al. 2019). We circularly distributed zero-mass test particles throughout the HD 3651 system at 21 logarithmically spaced values of semimajor axis. Orbits ranged from $(1 - e)/2$ to $2(1 + e)$ times the semimajor axis of HD 3651 b. The simulation was integrated with 1 day timesteps for 10 Myr, with post-Newtonian precessional effects (Nobili & Roxburgh 1986; Tamayo et al. 2020) taken into account. Particles that collided with the planet or host star were removed from the simulation. The outcomes are depicted in Figure 5. HD 3651 b clears out most particles within and slightly outside of its orbit, as expected from stability theory (e.g., Gladman 1993). Exceptions tend to be in mean-motion resonance with the planet, but their orbits are significantly disturbed. Although some particles survive within ~ 0.09 au, their orbits are disturbed by the planet as seen by fractional changes in semimajor axis. Remaining particles may not last on longer timescales; indeed, a few particles within this boundary were cleared out within 10 Myr. If a close-in Earth-mass planet could survive, it would leave a semi-amplitude signature of no more than ~ 34 cm s $^{-1}$. This value is above our measurement precision, however, our sampling might not be sufficient for such a planet to be detectable in the periodogram. More massive or closer-in planets would leave more significant signals.

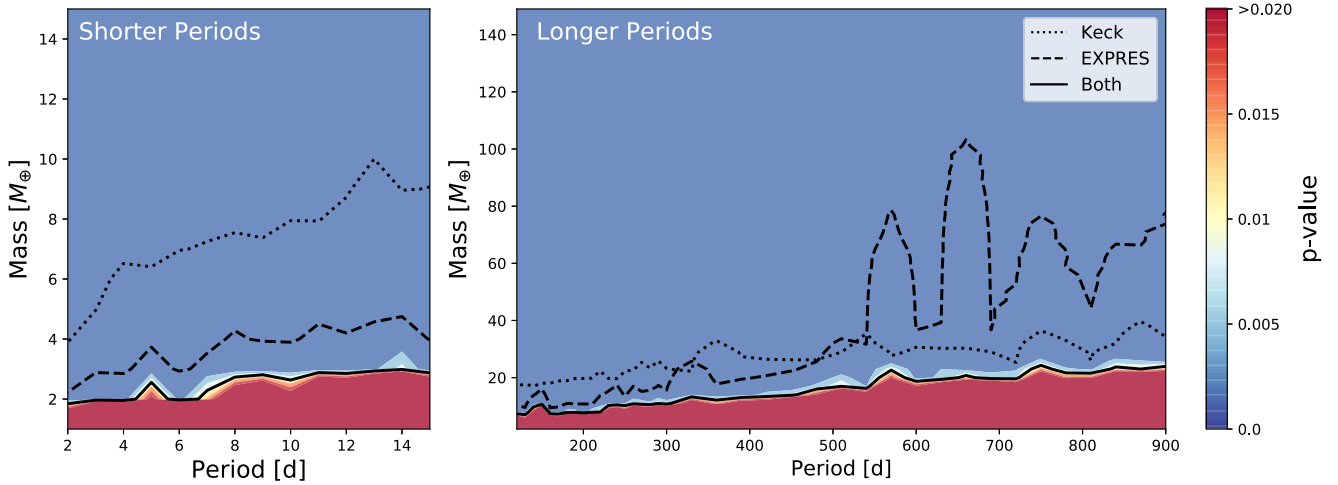


Figure 6. P -value contours with respect to mass and period showing the significance at which a planet would have been detected using the Keck HIRES and EXPRES data separately and together. With a p -value of less than 0.01 considered a successful detection, the black solid line marks the border of detectability. The detectability border when using just HIRES data or just EXPRES data is shown as dotted and dashed lines, respectively. The left plot shows shorter periods while the right plot investigates longer periods. Planets at the intervening periods would have been cleared out by HD 3651b’s orbit (see Figure 5).

5.1. Detectability Limits

Given the potential for at least marginally stable orbits at very short periods, we ran simulations to place mass limits on planets that might remain undetected with the data at hand. From the dynamics, planets within 0.09 au of the host star, or with less than 11 day orbits, may survive. We therefore simulate possible planets out to 15 day periods and up to 15 Earth masses.

For each planet, we simulate Keplerian RVs with identical temporal sampling as the observed data sets, preserving any window functions in the observations. Representative white and red noise is added, scaled to the rms of each data set’s planet fit and the calculated activity level of HD 3651 respectively. For each simulated planet, 1500 independent realizations of noise are generated. We then compare the periodogram power of just the noise against the periodogram power of the noise with the injected RV signal at the injected period.

The p -value for each simulated planet gives the probability that the noise has equally or more significant signal as the injected signal plus noise, meaning the injected signal was buried in the noise. A p -value of less than 0.01 is deemed a successful detection. The results are shown in Figure 6, where contours are drawn in p -value space. Blue areas indicate that if such a planet existed, it would have already been detected. Only planets smaller than two or three Earth masses may still be hidden in the data.

Although we are most concerned about short-period signals, our dynamical simulations also showed possible stable orbits beyond the 2:1 mean-motion resonance of HD 3651 b. We performed the same detectability simulations as above for periods between 120 and 900 days with planet masses of $2M_{\oplus} \leq M \leq 150M_{\oplus}$ (see Figure 5 right). We find that planets with masses above $6M_{\oplus}$ are excluded out to 160 days, $M > 8M_{\oplus}$ is excluded out to 210 days, and $M > 10$ is excluded out to 300 days. There is a window near 150 days where a lack of the higher cadence EXPRES data would permit planets up to $10M_{\oplus}$ to remain undetected. All planets above $25M_{\oplus}$ are excluded out to 900 day orbits. The higher precision of EXPRES allows the EXPRES data to exclude more short-period planets with lower masses than even the 20 yr time

baseline of the HIRES data. However, as expected, the long time baseline of Keck data surpasses the 4 month time baseline of EXPRES data for orbital periods longer than a year.

6. Conclusions

The EXPRES 100 Earths Survey has completed its first year of science operations. The instrumental precision of EXPRES has been measured to be 10 cm s^{-1} (Blackman et al. 2020) and the single-measurement precision on stars is about 30 cm s^{-1} for spectra with S/N of 250 per pixel near 550 nm (Petersburg et al. 2020). In addition to instrumental errors, we expect that other contributors to the RV error budget will include photospheric velocities, undetected low-mass planets in short-period orbits, telluric contamination, and errors from our analysis methods.

To eliminate some of the possible terms in the EPRV error budget we have used a new benchmark: the chromospherically quiet HD 3651 star, which hosts an eccentric, Saturn-mass planet in a ~ 62 day orbit. We carried out N -body simulations to demonstrate that planets interior to the Saturn-mass planet, HD 3651 b, would be dynamically unstable; this eliminates undetected short-period, low-mass planets as one possible source of RV scatter in our data. The rms scatter after fitting a Keplerian model is 58 cm s^{-1} over ~ 6 months. This suggests that added (roughly in quadrature) to our single-measurement errors of 30 cm s^{-1} , the remaining error terms (stellar activity, imperfectly modeled telluric contamination, and long-term instrumental drifts) contribute no more than about 50 cm s^{-1} . The residuals to this single-planet fit give a good measure of the true long-term RV precision for chromospherically quiet stars observed with EXPRES. If similarly quiet stars exhibit more than 50 cm s^{-1} RV scatter, then undetected, short-period planets are good candidates for those RV variations.

Importantly, the result that the intrinsic long-term precision for chromospherically quiet stars is $\sim 50 \text{ cm s}^{-1}$ helps to answer the question of whether RV precision in previous-era spectrographs was limited by the instrument, the analysis methods, or stability of the stellar photosphere. Several astronomers have long argued that photospheric velocities were the tall pole in the RV error budget. However, this work shows that in the case of quiet stars, the photospheric velocities




were not dominating the error budget and this is validation for our decade-long effort to design EXPRES as a next-generation EPRV spectrograph. While it is certainly true that photospheric velocities from active stars will be a strong contributor to the RV error budget, it is also likely that the high-fidelity data from next-generation EPRV spectrographs offer the best chance for ultimately disentangling those photospheric velocities. The EPRV spectrographs will help the community to take the next big step along the path toward detecting smaller amplitude signals. This is a new parameter space for RV surveys. The statistical results from the Kepler mission suggest that this new parameter space will be a rich source of previously undetected exoplanets.

EXPRES is not the only new EPRV instrument, and users of other EPRV spectrographs will want to evaluate their on-sky precision to track down instrumental issues that may affect their planet detection capability. HD 3651 b is an ideal benchmark for demonstrating long-term precision and for showing improvements relative to EXPRES. At a moderate northern decl., the star is observable by all current EPRV spectrographs and its brightness makes it an ideal standard for comparing RV precision and instrumental stability.

These results made use of the Lowell Discovery Telescope at Lowell Observatory. Lowell is a private, non-profit institution dedicated to astrophysical research and public appreciation of astronomy and operates the LDT in partnership with Boston University, the University of Maryland, the University of Toledo, Northern Arizona University, and Yale University. We thank Lowell astronomer, Maxime Devogele, for generously yielding telescope time so that we could obtain the radial velocity point for HD 3651 b near periastron passage. We gratefully acknowledge ongoing support for telescope time from Yale University, the Heising-Simons Foundation, and an anonymous donor in the Yale community. We especially thank the NSF for funding that allowed for precise wavelength calibration and software pipelines through NSF ATI-1509436 and NSF AST-1616086 and for the construction of EXPRES through MRI-1429365. G.W.H. acknowledges long-term support from NASA, NSF, Tennessee State University, and the State of Tennessee through its Centers of Excellence program. This material is based upon work supported by the National Science Foundation Graduate Research Fellowship under grant No. DGE1122492 (R.R.P., L.L.Z., and A.B.D.).

ORCID iDs

John M. Brewer  <https://orcid.org/0000-0002-9873-1471>
Debra A. Fischer  <https://orcid.org/0000-0003-2221-0861>

Ryan T. Blackman  <https://orcid.org/0000-0002-0303-3276>
Allen B. Davis  <https://orcid.org/0000-0002-5070-8395>
Gregory Laughlin  <https://orcid.org/0000-0002-3253-2621>
J. M. Joel Ong
(冕王加)  <https://orcid.org/0000-0001-7664-648X>
Ryan R. Petersburg  <https://orcid.org/0000-0003-2168-0191>
Andrew E. Szymkowiak  <https://orcid.org/0000-0002-4974-687X>
Lily L. Zhao  <https://orcid.org/0000-0002-3852-3590>
Gregory W. Henry  <https://orcid.org/0000-0003-4155-8513>
Joe Llama  <https://orcid.org/0000-0003-4450-0368>

References

- Blackman, R. T., Fischer, D. A., Jurgenson, C. A., et al. 2020, *AJ*, **159**, 238
Blackman, R. T., Ong, J. M. J., & Fischer, D. A. 2019, *AJ*, **158**, 40
Blackman, R. T., Szymkowiak, A. E., Fischer, D. A., & Jurgenson, C. A. 2017, *ApJ*, **837**, 18
Brems, S. S., Kürster, M., Trifonov, T., Reffert, S., & Quirrenbach, A. 2019, *A&A*, **632**, A37
Burke, C. J., Christiansen, J. L., Mullally, F., et al. 2015, *ApJ*, **809**, 8
Butler, R. P., Vogt, S. S., Laughlin, G., et al. 2017, *AJ*, **153**, 208
Chaplin, W. J., Cegla, H. M., Watson, C. A., Davies, G. R., & Ball, W. H. 2019, *AJ*, **157**, 163
Cosentino, R., Lovis, C., Pepe, F., et al. 2014, *Proc. SPIE*, **9147**, 91478C
DeGroot, W. T., Levine, S. E., Bida, T. A., et al. 2014, *Proc. SPIE*, **9145**, 91452C
Fischer, D. A., Anglada-Escude, G., Arriagada, P., et al. 2016, *PASP*, **128**, 066001
Fischer, D. A., Butler, R. P., Marcy, G. W., Vogt, S. S., & Henry, G. W. 2003, *ApJ*, **590**, 1081
Giguere, M. J., Fischer, D. A., Howard, A. W., et al. 2012, *ApJ*, **744**, 4
Gladman, B. 1993, *Icar*, **106**, 247
Henry, G. W. 1999, *PASP*, **111**, 845
Hoeijmakers, H. J., Cabot, S. H. C., Zhao, L., et al. 2020, arXiv:2004.08415
Hsu, D. C., Ford, E. B., Ragozzine, D., & Morehead, R. C. 2018, *AJ*, **155**, 205
Huang, Y., Liu, X. W., Chen, B. Q., et al. 2018, *AJ*, **156**, 90
Isaacson, H., & Fischer, D. 2010, *ApJ*, **725**, 875
Jurgenson, C., Fischer, D., McCracken, T., et al. 2016, *Proc. SPIE*, **9908**, 99086T
Leet, C., Fischer, D. A., & Valenti, J. A. 2019, *AJ*, **157**, 187
Levine, S. E., Bida, T. A., Chylek, T., et al. 2012, *Proc. SPIE*, **8444**, 844419
Mayor, M., Pepe, F., Queloz, D., et al. 2003, *Msngr*, **114**, 20
Nobili, A., & Roxburgh, I. W. 1986, in IAU Symp. 114, *Relativity in Celestial Mechanics and Astrometry*, High Precision Dynamical Theories and Observational Verifications, ed. J. Kovalevsky & V. A. Brumberg (Dordrecht: D. Reidel), 105
Petersburg, R. R., McCracken, T. M., Eggerman, D., et al. 2018, *ApJ*, **853**, 181
Petersburg, R. R., Ong, J. M. J., Zhao, L. L., et al. 2020, *AJ*, **159**, 187
Probst, R. A., Lo Curto, G., Ávila, G., et al. 2016, *Proc. SPIE*, **9908**, 99086A
Rein, H., Hernandez, D. M., Tamayo, D., et al. 2019, *MNRAS*, **485**, 5490
Ricker, G. R., Winn, J. N., Vanderspek, R., et al. 2015, *JATIS*, **1**, 014003
Soubiran, C., Jasiewicz, G., Chemin, L., et al. 2018, *A&A*, **616**, A7
Tamayo, D., Rein, H., Shi, P., & Hernandez, D. M. 2020, *MNRAS*, **491**, 2885
Winn, J. N., & Fabrycky, D. C. 2015, *ARA&A*, **53**, 409
Wright, J. T., & Howard, A. W. 2009, *ApJS*, **182**, 205